PHYSICAL REVIEW B **90**, 161107(R) (2014)

Pressure variation of Rashba spin splitting toward topological transition in the polar semiconductor BiTeI

T. Ideue,[1] J. G. Checkelsky,[2] M. S. Bahramy,[1,3] H. Murakawa,[4] Y. Kaneko,[3] N. Nagaosa,[1,3] and Y. Tokura[1,3]
[1]*Department of Applied Physics, University of Tokyo, Tokyo 113-8656, Japan*
[2]*Department of Physics, Massachusetts Institute of Technology, Cambridge, Massachusetts 02139, USA*
[3]*RIKEN Center for Emergent Matter Science (CEMS), Wako, Saitama 351-0198, Japan*
[4]*Department of Physics, Osaka University, Toyonaka, Osaka 560-0043, Japan*
(Received 10 July 2014; revised manuscript received 8 October 2014; published 27 October 2014)

BiTeI is a polar semiconductor with gigantic Rashba spin-split bands in bulk. We have investigated the effect of pressure on the electronic structure of this material via magnetotransport. Periods of Shubunikov–de Haas (SdH) oscillations originating from the spin-split outer Fermi surface and inner Fermi surface show disparate responses to pressure, while the carrier number derived from the Hall effect is unchanged with pressure. The associated parameters which characterize the spin-split band structure are strongly dependent on pressure, reflecting the pressure-induced band deformation. We find the SdH oscillations and transport response are consistent with the theoretically proposed pressure-induced band deformation leading to a topological phase transition. Our analysis suggests the critical pressure for the quantum phase transition near $P_c = 3.5$ GPa.

DOI: 10.1103/PhysRevB.90.161107 PACS number(s): 71.18.+y, 71.20.−b, 71.70.Di, 71.70.Ej

The spin-orbit interaction (SOI) plays a central role in determining the behavior of electrons in solids. In addition to the SOI-related subjects of spintronics, such as generation, manipulation, and detection of spin information, there has recently been an intense focus on the effect of the SOI on the electronic band structure itself. In particular, an extremely large SOI in small gap semiconductors has been shown theoretically [1–4] and experimentally [5–7] to give rise to a new exotic state of matter known as the topological insulator (TI). As probed by numerous experiments including angle resolved photoemission spectroscopy (ARPES) [6,7] and magnetotransport [8–12], this bulk insulating phase hosts metallic surface states composed of spin-polarized Dirac fermions, attracting both fundamental and technological interest [13,14].

The spin texture in the momentum space of the TI surface state is analogous to a Rashba-type spin structure [15]. A Rashba-type structure can be expected in a system with broken inversion symmetry so that electrons are subject to an effective SOI driven k-dependent Zeeman field perpendicular to both the polar axis and crystal momentum [15]. This effect in TIs and other Rashba-type materials lifts spin degeneracy in the Fermi surface, resulting in a chiral spin texture. Historically, this effect has been studied in surface [16–18] and interface [19] systems and more recently for the surface of TIs [20], where such a breaking of inversion symmetry naturally arises. More recently, a bulk (three-dimensional) polar semiconductor BiTeI has been shown to host a large Rashba-type spin-split bulk band structure [21]. Similar to the case of TIs, ARPES [21–24] and magnetotransport [25–27] have identified several salient features that point to the unique role of SOI in the electronic properties of these materials. It is widely expected that more exotic phases may exist also at the nexus of such bulk polar materials.

It was recently predicted by first-principles calculations that BiTeI shows a topological transition under pressure [28]. Figure 1 shows the evolution of the band structure of BiTeI with the application of pressure. At ambient pressure, the system shows a large Rashba spin-split band structure with an observed Rasba energy $E_R \sim 0.1$ eV and Rashba parameter $\alpha_R = 3.85$ eV Å for the conduction band. When the pressure is increased to a critical value P_c, the conduction band minimum and valence band top touch at the special k point along the $k_x(A - H)$ direction in the Brillouin zone. In this condition, the band gap collapses and a zero gap semimetallic state appears. Under higher pressure, the band gap reopens by inverting the valence and conduction band characters and the system enters the TI phase. From the calculations, it appears that the maximal cross-sectional area of both the inner Fermi surface (IFS) and outer Fermi surface (OFS) moves away from the $k_z = \pi/c$ plane just prior to the critical pressure. This TI phase is unique; it lacks inversion symmetry so that symmetry broken surface states with emergent magnetotransport phenomena are expected [28].

In recent years, there have been several reports on the experimental properties of this material under pressure, yet the topological transition and the related P_c have remained elusive. In experiments of x-ray powder diffraction and infrared spectroscopy, the lattice parameter ratio c/a shows a minimum between 2.0 and 2.9 GPa and the infrared spectra reveal a maximum in optical spectral weight of the charge carriers [29], though there was no clear evidence in the other infrared study under pressure [30]. Another report on an x-ray diffraction experiment estimated a topological transition point near 4.5 GPa [31]. To clarify the situation, we have studied the pressure effect on Shubunikov–de Haas (SdH) oscillations to directly trace the pressure-induced change of the Fermi surfaces of the Rashba spin-split bands and to elucidate the critical pressure at which topological transition occurs.

Single crystals of BiTeI were prepared by the Bridgman method. By means of powder x-ray diffraction, we have confirmed that these samples are single phase. The sample was cut to 1.75 mm × 1.5 mm × 175 μm. Ti(10 nm)/Au(50 nm) was deposited on the sample as the electrodes and gold wires were attached by silver paste. A piston-cylinder pressure cell was used for applying hydrostatic pressure with the use of Daphne 7474 as the pressure-transmitting medium, and the

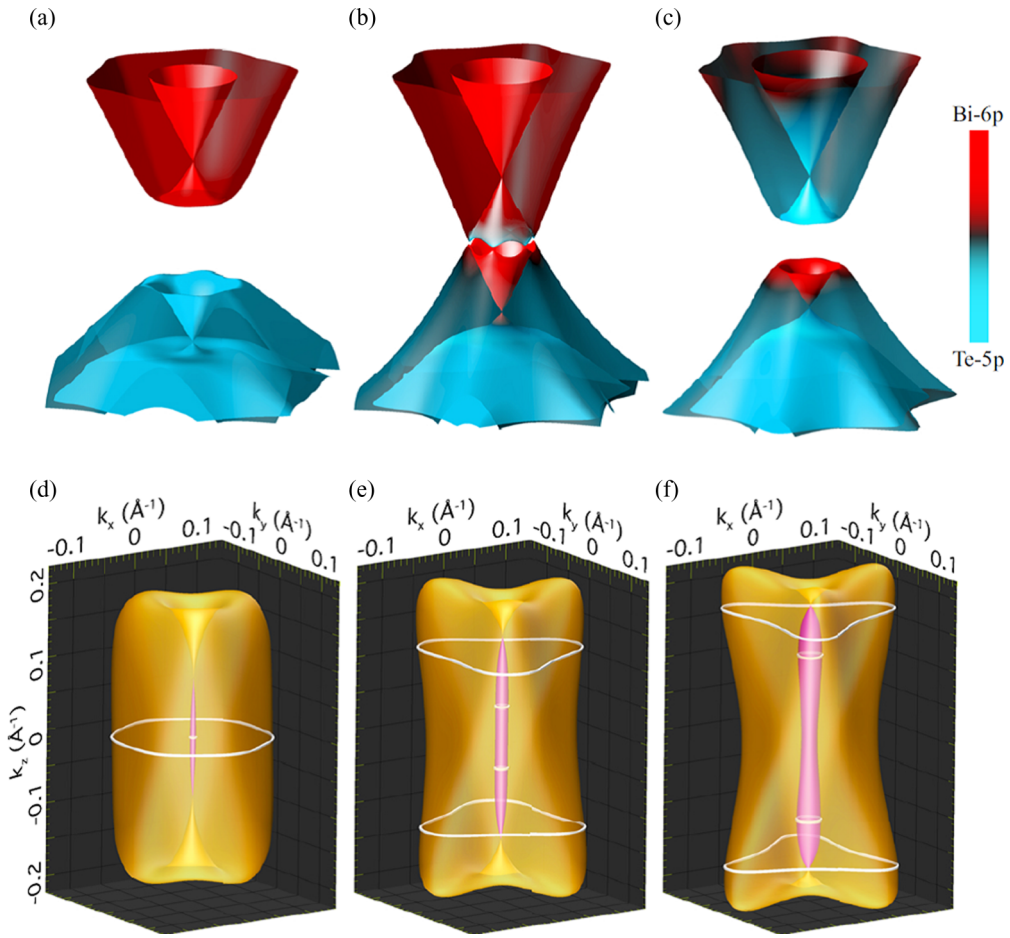

FIG. 1. (Color online) (a)–(c) Band structure and (e)–(f) three-dimensional Fermi surface of BiTeI under pressure. The red and blue colors in (a)–(c) correspond to Bi-6p and Te-5p orbital characters, respectively, and the enclosed area in (d)–(f) indicates the maximal cross-sectional area of each Fermi surface. P_c is the critical pressure for band inversion. (a), (d) $P \leqslant P_c$; (b), (e) $P = P_c$; (c), (f) $P \geqslant P_c$.

resistivity and Hall effect were measured with the use of a physical property measurement system (Quantum Design, Inc.). Measurements were performed in magnetic fields up to 14 T and under pressures up to 3 GPa.

The pressure dependences of longitudinal resistivity ρ_{xx} and Hall resistivity ρ_{yx} are shown in Fig. 2. The electron concentration in the measured sample is estimated as 4.6×10^{19} cm^{-3} from the Hall effect at $T = 2$ K. This remains unchanged with the application of pressure [see the inset to Fig. 2(a)]. This carrier density suggests that the Fermi level is (by 42 meV at ambient pressure) above the Dirac point of the spin-split Rashba band structure; the calculated carrier concentration is $n \sim 2.9 \times 10^{19}$ cm^{-3} when the Fermi level E_F is at the Dirac point of the conduction band. In contrast to the pressure-independent ρ_{yx}, ρ_{xx} is steadily reduced with increasing pressure.

Figure 2(b) shows the magnetic field dependence of ρ_{xx} at several pressures. The magnetic field was applied up to 14 T along the c axis. Mobility estimated by using the relation of $\sigma_{xx}(B) = \sigma_{xx}(0)/[1 + (\mu B)^2]$ and the value of conductivity at $B = 14$ T increases monotonically with pressure from $\mu \sim 450$ cm^2/V s at ambient pressure to $\mu \sim 570$ cm^2/V s at $P = 3$ GPa. This increase is consistent with the behavior of the low-field mobility value calculated by $\mu_0 = \sigma_{xx}(B = 0)/ne$, indicating the reduction of cyclotron mass or scattering rate by pressure.

In addition, ρ_{xx} shows clear SdH oscillations with two different periods with $1/B$, as also reported in previous studies at ambient pressure [25–27]. Oscillations with a longer period in the low magnetic field region correspond to IFS, and those with a shorter period in the high-field region originate from OFS [Fig. 2(c)]. Oscillatory components in the low magnetic field region ($B \leqslant 10$ T) and high magnetic field region ($B \geqslant 10$ T) are extracted by subtracting a polynominal background and are shown in Figs. 2(d) and 2(e). The data are shifted vertically in proportion to the value of pressure. The peaks of each oscillatory component associated with the same Landau index are connected by dashed lines. In contrast to the Hall resistivity, SdH oscillations are strongly dependent on pressure; the period of IFS oscillations becomes shorter with the increase of pressure while that of OFS oscillation is elongated by application of pressure.

The evolution of the SdH oscillations can be clearly seen also in the Landau fan diagram (Fig. 3). In this plot, we assign integer indices to the ρ_{xx} peak position in $1/B$ and half-integer indices to the ρ_{xx} valley positions, following the procedure adopted in a previous work [25]. Due to the negligible Zeeman splitting, the linearity of the index plot holds well also under

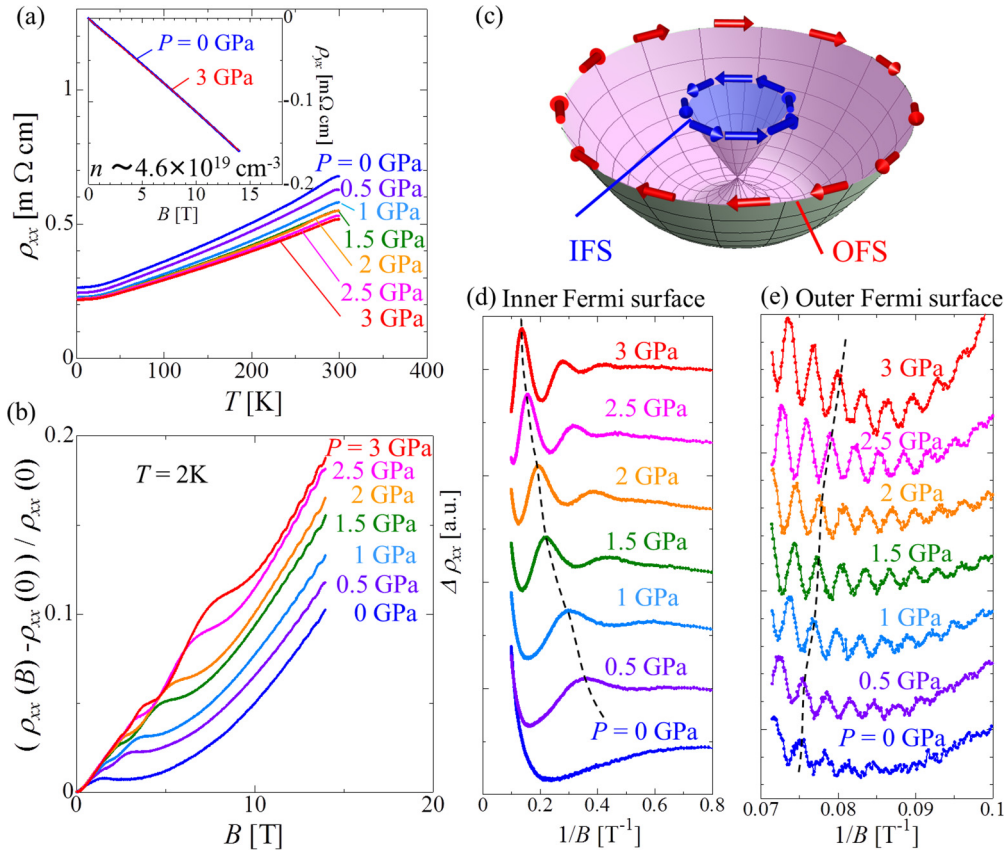

FIG. 2. (Color online) (a), (b), (d), (e) Pressure dependence of longitudinal resistivity and Hall resistivity. (a) Temperature dependence of ρ_{xx} under pressure. The inset shows Hall resistivity at $T = 2$ K under each pressure. ρ_{yx} and the associated carrier number remain unchanged by pressure. (b) Magnetic field dependence of ρ_{xx} at $T = 2$ K under each pressure. (c) Inner Fermi surface and outer Fermi surface of a Rashba spin-split band. (d), (e) Oscillatory components of ρ_{xx} in a (d) low-field and (e) high-field region.

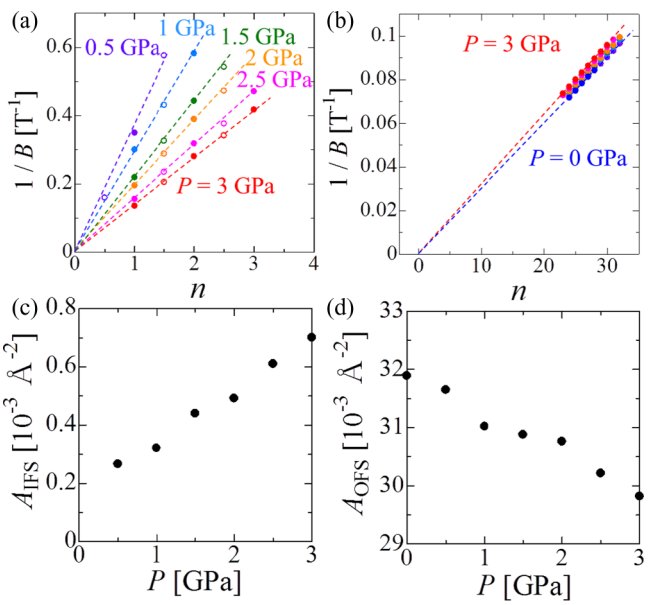

FIG. 3. (Color online) Landau index plot of (a) IFS oscillations and (b) OFS oscillations. Solid circles indicate the integer index (ρ_{xx} peak), and open circles denote the half-integer index (ρ_{xx} valley). Pressure dependence of the extremal cross-sectional area of (c) IFS and (d) OFS.

the pressure. The slope (oscillation period) of the line gives the extremal cross-sectional area of each Fermi surface via the relation

$$A_{\mathrm{OFS}} = \frac{2\pi e}{\hbar \triangle_{\mathrm{OFS}}(1/B)}, \quad A_{\mathrm{IFS}} = \frac{2\pi e}{\hbar \triangle_{\mathrm{IFS}}(1/B)}. \tag{1}$$

Here A_{OFS} and A_{IFS} are the extremal Fermi surface areas with periods (slopes of the Landau index plot) $\triangle_{\mathrm{OFS}}(1/B)$ and $\triangle_{\mathrm{IFS}}(1/B)$. Figures 3(c) and 3(d) show the calculated cross-sectional area of IFS and OFS. With the application of pressure, the IFS is expanded while OFS slightly shrinks.

To probe the topological phase transition, we have further analyzed the results in the following way. If the system is an ideal two-dimensional system, we can neglect the dispersion along the c axis and the cubic Rashba term, so that the effective Hamiltonian can be written

$$H = \frac{\hbar^2\left(k_x^2 + k_y^2\right)}{2m^*} + \alpha(k_x\sigma_y - k_y\sigma_x), \tag{2}$$

where m^* is the effective mass, α the Rashba parameter, and σ_x, σ_y the Pauli matrices for the spin degrees of freedom. This leads to the simple relation of the Fermi wave numbers of OFS and IFS,

$$k_{\mathrm{OFS}} - k_{\mathrm{IFS}} = \frac{2\alpha m^*}{\hbar^2}. \tag{3}$$

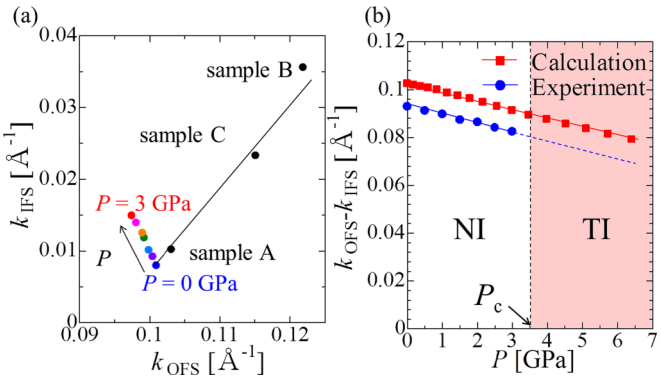

FIG. 4. (Color online) (a) (k_{OFS},k_{IFS}) plots of k_{OFS} and k_{IFS} for the present measured sample and their pressure dependence. Points for samples A, B, and C in a previous work [25] are also plotted. (b) Comparison of $k_{OFS} - k_{IFS}$ values between experiment and calculation. NI and TI stand for the nontopological and topological insulator, respectively, and P_c for the theoretically predicted critical pressure of the topological transition [28].

This relation has the remarkable characteristic that it is independent of carrier density. In other words, if the structural parameters of a two-dimensional Rashba system α and m^* are fixed, the difference between the Fermi wave numbers of OFS and IFS is constant regardless of the chemical potential. To examine this relation, Fermi wave numbers are calculated by

$$k_{OFS} = \sqrt{\frac{A_{OFS}}{\pi}}, \quad k_{IFS} = \sqrt{\frac{A_{IFS}}{\pi}}, \tag{4}$$

and are plotted in Fig. 4(a). We have also plotted the values obtained from other experiments (samples A, B, and C) in a previous work [25]. Data points at ambient pressure are roughly on the universal line of slope 1, which shows that Eq. (3) with the approximation of a simple two-dimensional Rashba model holds well. Furthermore, we can see that the points of (k_{OFS},k_{IFS}) show a systematic change with pressure and clearly deviate from the universal line obtained at ambient pressure. This is direct evidence of pressure-induced band deformation as the value of $k_{OFS} - k_{IFS}$ corresponds to the band parameters through Eq. (3). Modulation of the atomic distances under pressure alters the electronic potentials and SOI, which are directly related to the effective mass and Rashba parameter.

In Fig. 4(b), we compare the experimentally obtained values of $k_{OFS} - k_{IFS}$ as a function of pressure with those by the first-principles calculations [32]. The trends in the experiments and calculations are in reasonable agreement. Values of $k_{OFS} - k_{IFS}$ decrease linearly with pressure and the magnitude of the decrease (slope of the lines) coincides with each other. This implies that pressure-induced band deformation likely drives the system close to the topologically nontrivial phase near $P = 3.5$ GPa, as the calculation predicted [28]. Importantly, both theory and experiment show no anomaly around the topological transition. This is perhaps because the Fermi level in this sample is far (by 154 meV at ambient pressure) above the conduction band minimum. In addition, application of pressure promotes the mixing of p_z orbitals of Bi and Te (as shown in Fig. 1), thereby modifying the band dispersions in the whole Brillouin zone and especially along the c axis. The application of pressure is also expected to modify the cubic and higher k terms in the spin-split Hamiltonian, which is neglected in the above simple treatment by Eq. (3).

There is still a small difference of $k_{OFS} - k_{IFS}$ values between calculations and experiments, which is attributed to the natural shortcoming of the density functional theory approaches in treating the exchange-correlation potentials. Despite this small difference, the trend of pressure-induced change is very similar between the experiments and calculations. Accordingly, we expect that the pressure-induced band deformation scenario for a topological transition is viable as well as the predicted value (∼3.5 GPa) of the critical pressure. To extract more information about the topological transition, experiments using a sample with a much lower carrier concentration would be needed.

In summary, we have studied the pressure effect on Rashba spin splitting in a polar semiconductor BiTeI. SdH oscillations with two distinct periods corresponding to the inner and outer Fermi surfaces strongly depend on the pressure, reflecting the band deformation, while the carrier number remains unchanged under pressure. The Fermi wave numbers associated with respective spin-split Fermi surfaces, whose parameters are modified with pressure, can be well described by a simple linear Rashba model as the system approaches the topologically nontrivial phase.

Note added. Recently, we become aware of a related pressure study by Van Gennep *et al.* [33].

The authors thank L. D. Ye and N. Kanawzawa for fruitful discussions. This work was supported by Grants-in-Aid for Scientific Research (S) (No. 24224009) from the Ministry of Education, Culture, Sports, Science and Technology (MEXT) of Japan and the Funding Program for World-Leading Innovative R&D on Science and Technology (FIRST Program).

[1] C. L. Kane and E. J. Mele, Phys. Rev. Lett. **95**, 146802 (2005).
[2] B. A. Bernig, T. L. Hughes, and S. C. Zhang, Science **314**, 1757 (2006).
[3] L. Fu and C. L. Kane, Phys. Rev. B **76**, 045302 (2007).
[4] H. Zhang, C. X. Liu, X. L. Qi, X. Dai, Z. Fang, and S. C. Zhang, Nat. Phys. **5**, 438 (2009).
[5] M. König, S. Wiedmann, C. Brüne, A. Roth, H. Buhmann, L. W. Molenkamp, X. L. Qi, and S. C. Zhang, Science **318**, 766 (2007).
[6] D. Hsieh, D. Qian, L. Wray, Y. Xia, Y. S. Hor, R. J. Cava, and M. Z. Hasan, Nature (London) **452**, 970 (2008).
[7] Y. Xia, D. Qian, D. Hsieh, L. Wray, A. Pal, H. Lin, A. Bansil, D. Grauer, Y. S. Hor, R. J. Cava, and M. Z. Hasan, Nat. Phys. **5**, 398 (2009).
[8] P. Cheng, C. Song, T. Zhang, Y. Zhang, Y. Wang, J. F. Jia, J. Wang, Y. Wang, B. F. Zhu, X. Chen, X. Ma, K. He, L. Wang, X. Dai, Z. Fang, X. Xie, X. L. Qi, C. X. Liu, S. C. Zhang, and Q. K. Xue, Phys. Rev. Lett. **105**, 076801 (2010).

[9] T. Hanaguri, K. Igarashi, M. Kawamura, H. Takagi, and T. Sasagawa, Phys. Rev. B **82**, 081305(R) (2010).
[10] D. X. Qu, Y. S. Hor, J. Xiong, R. J. Cava, and N. P. Ong, Science **329**, 821 (2010).
[11] J. G. Analytis, R. D. McDonald, S. C. Riggs, J. H. Chu, G. S. Boebinger, and I. R. Fisher, Nat. Phys. **6**, 960 (2010).
[12] R. Yoshimi, A. Tsukazaki, K. Kikutake, J. G. Checkelsky, K. S. Takahashi, M. Kawasaki, and Y. Tokura, Nat. Mater. **13**, 253 (2014).
[13] M. Z. Hasan and C. L. Kane, Rev. Mod. Phys. **82**, 3045 (2010).
[14] X. L. Qi and S. C. Zhang, Rev. Mod. Phys. **83**, 1057 (2011).
[15] E. I. Rashba, Sov. Phys. Solid State **2**, 1109 (1960).
[16] S. LaShell, B. A. McDougall, and E. Jensen, Phys. Rev. Lett. **77**, 3419 (1996).
[17] C. R. Ast, J. Henk, A. Ernst, L. Moreschini, M. C. Falub, D. Pacilé, P. Bruno, K. Kern, and M. Grioni, Phys. Rev. Lett. **98**, 186807 (2007).
[18] Y. M. Koroteev, G. Bihlmayer, J. E. Gayone, E. V. Chulkov, S. Blügel, P. M. Echenique, and Ph. Hofmann, Phys. Rev. Lett. **93**, 046403 (2004).
[19] J. Nitta, T. Akazaki, H. Takayanagi, and T. Enoki, Phys. Rev. Lett. **78**, 1335 (1997).
[20] M. S. Bahramy, P. D. C. King, A. de la Torre, J. Chang, M. Shi, L. Patthey, G. Balakrishnan, Ph. Hofmann, R. Arita, N. Nagaosa, and F. Baumberfer, Nat. Commun. **3**, 1159 (2012).
[21] K. Ishizawa, M. S. Bahramy, H. Murakawa, M. Sakano, T. Shimojima, T. Sonobe, K. Koizumi, S. Shin, H. Miyahara, A. Kimura, K. Miyamoto, T. Okuda, H. Namatame, M. Taniguchi. R. Arita, N. Nagaosa, K. Kobayashi, Y. Murakami, R. Kumai, Y. Kaneko, Y. Onose, and Y. Tokura, Nat. Mater. **10**, 521 (2011).
[22] G. Landolt, S. V. Eremeev, Y. M. Koroteev, B. Slomski, S. Muff, T. Neupert, M. Kobayashi, V. N. Strocov, T. Schmitt, Z. S. Aliev, M. B. Babanly, I. R. Amiraslanov, E. V. Chulkov, J. Osterwalder, and J. H. Dil, Phys. Rev. Lett. **109**, 116403 (2012).
[23] A. Crepaldi, L. Moreschini, G. Autès, C. Tournier-Colletta, S. Moser, N. Virk, H. Berger, Ph. Bugnon, Y. J. Chang, K. Kern, A. Bostwick, E. Rotenberg, O. V. Yazyev, and M. Grioni, Phys. Rev. Lett. **109**, 096803 (2012).
[24] M. Sakano, M. S. Bahramy, A. Katayama, T. Shimojima, H. Murakawa, Y. Kaneko, W. Malaeb, S. Shin, K. Ono, H. Kumigashira, R. Arita, N. Nagaosa, H. Y. Hwang, Y. Tokura, and K. Ishizaka, Phys. Rev. Lett. **110**, 107204 (2013).
[25] H. Murakawa, M. S. Bahramy, M. Tokunaga, Y. Kohama, C. Bell, Y. Kaneko, N. Nagaosa, H. Y. Hwang, and Y. Tokura, Science **342**, 1490 (2013).
[26] C. Bell, M. S. Bahramy, H. Murakawa, J. G. Checkelsky, R. Arita, Y. Kaneko, Y. Onose, M. Tokunaga, Y. Kohama, N. Nagaosa, Y. Tokura, and H. Y. Hwang, Phys. Rev. B **87**, 081109(R) (2013).
[27] C. Martin, E. D. Mun, H. Berger, V. S. Zapf, and D. B. Tanner, Phys. Rev. B **87**, 041104(R) (2013).
[28] M. S. Bahramy, B.-J. Yang, R. Arita, and N. Nagaosa, Nat. Commun. **3**, 679 (2012).
[29] X. Xi, C. Ma, Z. Liu, Z. Chen, W. Ku, H. Berger, C. Martin, D. B. Tanner, and G. L. Carr, Phys. Rev. Lett. **111**, 155701 (2013).
[30] M. K. Tran, J. Levallois, P. Lerch, J. Teyssier, A. B. Kuzmenko, G. Autès, O. V. Yazyev, A. Ubaldini, E. Giannini, D. van der Marel, and A. Akrap, Phys. Rev. Lett. **112**, 047402 (2014).
[31] Y. Chen, X. Xi, W. L. Yim, F. Peng, Y. Wang, H. Wang, Y. Ma, G. Liu, C. Sun, C. Ma, Z. Chen, and H. Berger, J. Phys. Chem. C. **117**, 25677 (2013).
[32] Volume optimization calculations were carried out using the projected augmented wave method and improved Perdew-Burke-Ernzerhof functional for solids (PBEsol), as implemented in the VASP program [G. Kresse and J. Furthmüller, Phys. Rev. B **54**, 11169 (1996); G. Kresse *et al.*, Vienna Ab initio Software Packages (VASP) version 5.3.3, http://cms.mpi.univie.ac.at/vasp/]. The cutoff energy for plane waves was set to 500 eV and the Brillouin zone was sampled by a $20 \times 20 \times 20k$ mesh. At each pressure, both the atomic positions and lattice parameters were fully optimized until the magnitude of force on each ion became less than 0.001 eV/Å. Using the optimized structural parameters, the electronic structure at each pressure was subsequently calculated within the same level of PBEsol theory using the augmented plane wave plus atomic orbitals method, as implemented in the WIEN2K program (P. Blaha, K. Schwarz, G. Madsen, D. Kvasnicka, and J. Luitz, WIEN2K package, version 13.1, http://www.wien2k.at).
[33] D. Van Gennep, S. Maiti, D. Graf, S. W. Tozer, C. Martin, H. Berger, D. L. Maslov, and J. J. Hamlin, J. Phys.: Condens. Matter **26**, 342202 (2014).